

Preliminary Study on a Biocompatible Cellulose Waterborne Polyurethane Composite Membrane

Haoqiang Yuan,[†] Yongqiang Zhang,[†] and Zhenhua Xue^{*}Cite This: *ACS Omega* 2022, 7, 30849–30855

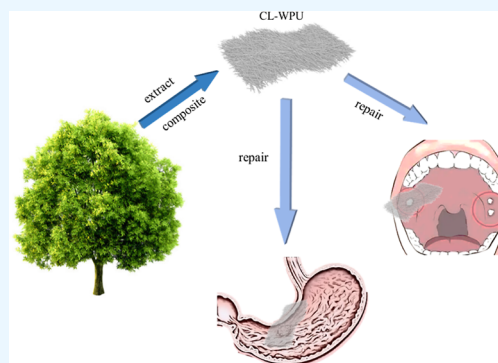
Read Online

ACCESS |

Metrics & More

Article Recommendations

ABSTRACT: A promising technique for repairing necrotic mucosa of human organs has emerged, in which composite films are used to replace human mucosa. In this work, neutral alpha-amylase corrosion solution with a concentration of 0.40 mg/mL and hydrochloric acid corrosion solution at pH 0.9 were used as simulated oral cavity and gastric fluid environments under the condition of human body temperature. The prepared cellulose film and the cellulose water-based polyurethane composite film (the concentration of water-based polyurethane was 90, 92, 94, 96, or 98%) were mixed in the simulated environment. The composite membrane had a weaker water swelling property (water swelling degree of 4.32%), weaker surface hydrophilicity (water contact angle of 59.05°), and stronger enzyme activity (1.77 U). This functional film composite material is expected to become an ideal substitute for human mucosa.



INTRODUCTION

Autologous organ mucosal transplantation is a common method to repair mucosal necrosis of human organs, but it has many limitations, such as insufficient donor source, need of additional incision, and so forth.^{1,2} In recent years, the necrotic mucosa of human organs has been replaced with other biological thin films, which increases the demand for biocompatible thin film materials.^{3–5} Cellulose (CL) and waterborne polyurethane (PU) have potential in this area because of their good biocompatibility.^{6,7}

CL exists in higher plants and some marine animals, algae, bacteria, and fungi.^{8,9} The annual output of recyclable CL is 100–150 billion tons, but only 2 million tons is used in production, accounting for 0.002% of the total output, which can be described as “inexhaustible”.¹⁰ Researchers at the Swiss Federal Laboratory for Testing and Research (Empa) developed CL membranes with antibacterial peptides that allow bacterial invasion of wounds and infection to be eliminated at an early stage.^{11,12} Li et al. (2021) prepared the first zeolitic imidazolate framework-90/laccase biocomposites. A novel CL membrane with biocatalytic function was prepared, which has good detection and degradation performance for phenolic pollutants.^{13,14}

PU is a polymer material; different types of PUs are obtained by adjusting the types of monomers, dosage ratio, and reaction conditions.¹⁵ As a viscoelastic damping material, PU is a key research object due to the corresponding changes in its structure and composition.¹⁶ To reduce the emissions of organic compounds, waterborne PU (WPU) has been developed. It retains the excellent properties of the traditional

solvent PU, but it also has some problems, such as poor water resistance.¹⁷ PU is a new type of biomaterial because of its good physiological adaptability, air permeability, water resistance, and moisture permeability; it can be used in industrial filter materials, fabric coatings, and biomedical fields.^{18,19} Recent research shows that many PU systems are suitable for medical stents.^{20,21}

The composite membrane prepared by mixing CL and WPU in a certain proportion can have the advantages of both materials according to the application requirements.^{22,23} In 2006, the composite of CNCs and PU was first reported.^{24–26} Pei et al. (2011) added 1% CNCs into the reacted PU prepolymer, and the prepared PU/CNCs composite had ultra-high tensile strength and elongation at break. Girouard et al. (2016) made use of the different reaction characteristics of two isocyanate functional groups of isophorone diisocyanate to prepare CNCs, which enhanced the interfacial bonding force between CNCs and PU matrix, maintained the elongation at break, and improved the dispersibility of CNCs.^{27,28}

CL and WPU composites are the subject of recent research.^{29–31} However, there are few studies on the preparation of composite films by compounding CL and WPU, and the research on the biocompatibility of the

Received: April 20, 2022

Accepted: August 5, 2022

Published: August 22, 2022



composite films is almost blank.^{32,33} This study reports the preparation of CL film and CL–WPU composite film. The concentration of WPU was 90, 92, 94, 96, or 98%. They were separately placed in simulated oral and gastric fluid environments (neutral α -amylase corrosion solution at a concentration of 0.40 mg/mL and hydrochloric acid corrosion solution at pH 0.9). Compared with the CL membrane, the composite membrane had weaker water-absorbing swelling property (water-absorbing swelling degree of 4.32%), surface hydrophilicity (water contact angle of 59.05°), and stronger enzyme activity (1.77 U). It is a promising functional film composite, providing a possibility for repairing necrotic mucosa of human organs as a replacement film.

EXPERIMENTAL SECTION

Materials. CL (100%) was provided by Hebei Bailing Weichao Fine Materials Co., Ltd (Hebei, China). WPU resin was obtained from Guangzhou Hensic New Material Co., Ltd (Guangdong, China). Alpha amylase was supplied by J&K Scientific (China) Corporation (Shanghai, China). Citric acid and soluble starch were purchased from T'jkemao Chemical Reagents Co., Ltd (Tianjin, China). Copper chloride was received from Xilong Chemical Co., Ltd (Guangdong, China). Potassium iodide (KI), iodine (I), hydrochloric acid (HCl), and disodium hydrogen phosphate ($\text{Na}_2\text{HPO}_4 \cdot 12\text{H}_2\text{O}$) were supplied by Tianjin Fuchen Chemical Reagents (Tianjin, China).

Preparation of CL Films. A total of 50 g of sodium hydroxide, thiourea, urea, and pure water with a mass ratio of 8.0:6.5:8.0:77.5 were placed in a 250 mL beater and stirred until the mixture was transparent. Next, 2.05 g of absolutely dried CL was evenly dispersed in the abovementioned liquid and then placed at $-20\text{ }^\circ\text{C}$. After freezing for 30 min, it was stirred at room temperature for 10 min. If there was still solid CL, it was frozen for an additional 15 min and then stirred at room temperature. The process was repeated until the CL was completely dissolved. The dissolved CL solution was centrifuged at 8000 rpm for 10 min to obtain transparent and viscous CL solution. The transparent and viscous CL solution was slowly poured into pure water and quickly stirred to make it flocculent; the floc is regenerated CL. The flocculent regenerated CL was washed to neutral and then pumped and filtered with a sand core filter to form a membrane, as shown in Figure 1. After vacuum drying, it was sealed for storage.

Preparation of CL–WPU Composite Films. A certain amount of water-based PU was placed in a 200 mL beaker, and then CL was added to disperse evenly. The mass concentrations of PU were 98, 96, 94, 92, and 90%, which were labeled as CL–WPU98, CL–WPU96, CL–WPU94, CL–WPU92, and CL–WPU90, respectively. The film was scraped to a constant thickness, and the composite film material was vacuum-dried.

Effect of CL Films and CL–WPU Composite Films on α -amylase Activity. A total of 0.04 g of α -amylase was dissolved with buffer solution, with a final volume of 100 mL. It was stored at $4\text{ }^\circ\text{C}$. The prepared film material was immersed in α -amylase etching solution and heated in a $37 \pm 3\text{ }^\circ\text{C}$ water bath to study the effect of lignocellulosic film material on α -amylase activity.

Scanning Electron Microscopy. The lignocellulosic film material was cut into $5 \times 5\text{ mm}$ samples and placed on the sample platform. After vacuum gold-plating for 1 min, the

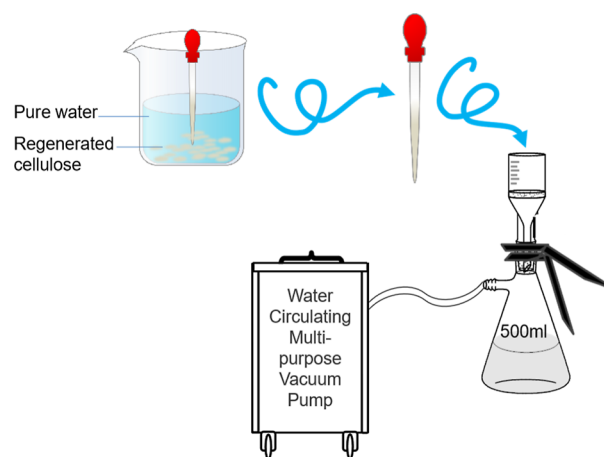


Figure 1. Simple flow chart for preparing CL films.

samples were placed into the scanning electron microscope (S-3400N, Phenom-World, Eindhoven, Netherlands) with an acceleration voltage of 0.3–30 kV.

FTIR Spectroscopic Analysis. The film was ground into powder, and 1–2 mg was evenly mixed with 200 mg of pure KBr powder. The film was pressed into thin sheets with a mold and kept at 8–10 MPa for 2 min. The sample was clamped into the fixture and placed on the fixed bracket in the instrument (TENSOR-27, Karlsruhe, Germany). The test range was $400\text{--}4000\text{ cm}^{-1}$.

Surface Hydrophilicity Testing. The water contact angle was used to evaluate the hydrophilicity of the material surface (V5 contact angle measuring instrument, Tianjin Yunfan Technology Co., LTD, Tianjin, China). The contact angle refers to the angle θ at the junction of solid, liquid, and gas phases, from the solid–liquid interface through the interior of the liquid to the gas–liquid. Usually, $\theta = 90^\circ$ is used as the boundary between hydrophilicity and hydrophobicity of the material surface. When the water contact angle $\theta > 90^\circ$, the surface is considered hydrophobic; otherwise, it is considered hydrophilic.

Water Absorption and Swelling Testing. The lignocellulosic membrane material was cut into a $30 \times 5\text{ mm}$ sample and freeze-dried to a constant re-denoted as m_0 . The sample was placed in deionized water and naturally expanded to a constant weight at $25\text{ }^\circ\text{C}$ and relative humidity of $99 \pm 1\%$, denoted as m_t . The equilibrium degree of swelling (Q_t) was calculated as follows.

$$Q_t = \frac{m_t - m_0}{m_0} \times 100\% \quad (1)$$

Corrosion Resistance Testing. The prepared α -amylase corrosion solution was a neutral solution with a concentration of 0.40 mg/mL, and the HCl corrosion solution was diluted to pH 0.9 with concentrated hydrochloric acid at pH 0.1. The prepared lignocellulosic membrane materials were completely immersed into the culture dishes containing α -amylase corrosion solution and HCl corrosion solution, respectively, and corroded at $37 \pm 3\text{ }^\circ\text{C}$ for 24 h. The effect of α -amylase etching solution and HCl etching solution on the corrosion resistance of membrane materials was studied.

Enzyme Activity Testing. The α -amylase activity was determined by a spectrophotometer. The same concentration of α -amylase solution and membrane material were added to a number of colorimetric tubes as sample tubes; buffer solution

was added to the colorimetric tubes as standard tubes. All tubes were kept in a 37 ± 3 °C water bath for 2 min, and an appropriate amount of 0.008 g/mL starch solution and 1 mL of termination solution were added under certain conditions. After shaking, the tubes were cooled to room temperature to determine their absorbance at 580 nm, as follows

$$\frac{m_x}{A_x} = \frac{m_s}{A_s} \quad (2)$$

$$m_x = \frac{m_s \times A_x}{A_s} \quad (3)$$

where m_e is the mass of α -amylase, m_x and A_x are the mass and absorbance of starch in the sample tube, respectively, and m_s and A_s are the mass and absorbance of standard starch, respectively.

The amount of starch in both the sample tube and the standard tube is 5 mL and 0.8% starch, namely, 40 mg. According to the abovementioned method, the amount of starch degradation in the sample tube is $(40 - m_x)$ mg. The enzyme activity λ and specific activity φ in the sample tube are calculated as follows.

$$\lambda = \frac{40 - m_x}{10} = \frac{40 - \frac{m_s \times A_x}{A_s}}{10} = 4 \left(1 - \frac{A_x}{A_s} \right) \quad (4)$$

$$\varphi = \frac{4 \left(1 - \frac{A_x}{A_s} \right)}{m_e} \quad (5)$$

Mechanical Testing. The mechanical properties of the film were tested using a 5940 universal mechanical testing machine (Instron, Norwood, MA, USA), with reference to the national standard GB/T 1040.3 (2006). The sample size was 30×5 mm, and the tensile test was carried out at room temperature at a speed of 10 mm/min. Each sample was repeated five times, and the average value was taken.

RESULTS AND DISCUSSION

Scanning Electron Microscopy. Figure 2f shows pure RC film materials with a relatively dense surface. The comparison of the six images shows that these lignocellulosic materials are evenly distributed in the composite film materials. With

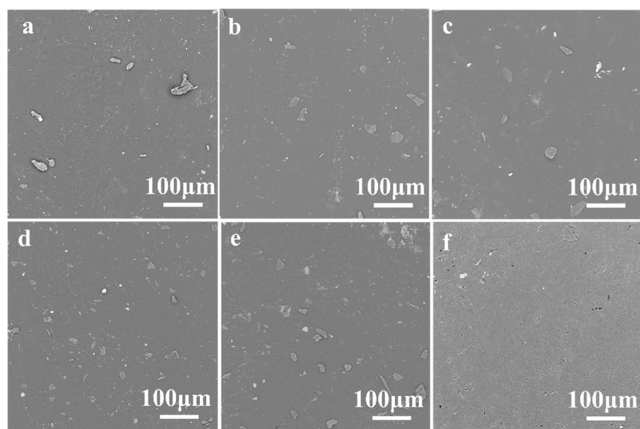


Figure 2. SEM images of different membrane materials without corrosion: (a) CL-WPU98; (b) CL-WPU96; (c) CL-WPU94; (d) CL-WPU92; (e) CL-WPU90; and (f) CL.

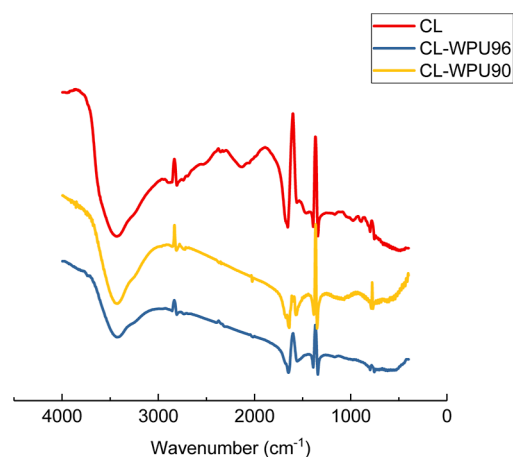


Figure 3. FTIR spectra of different composite membrane materials.

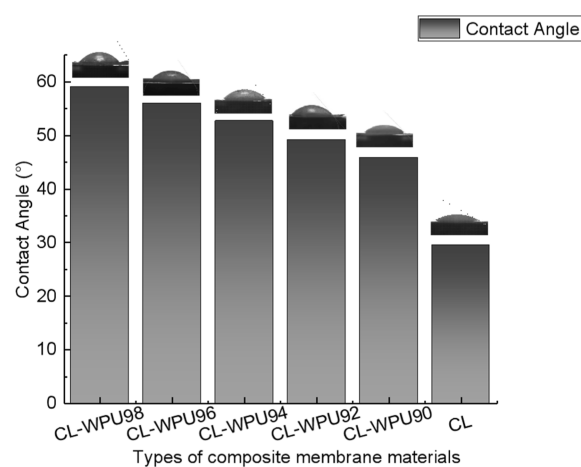


Figure 4. Contact angle between different membrane composite materials and water.

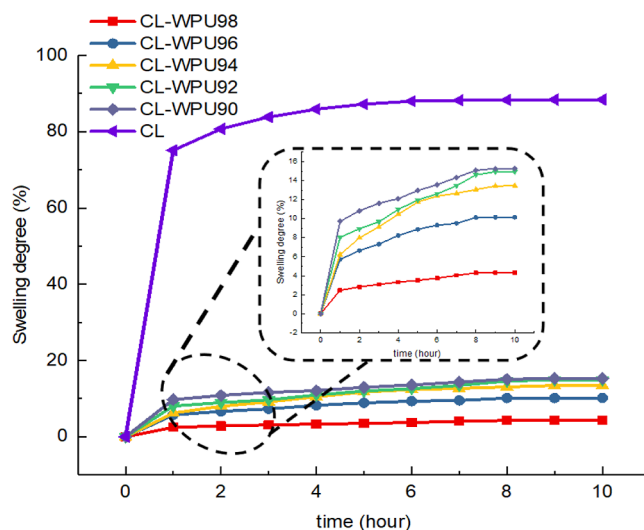


Figure 5. Change curve of the swelling degree of different membrane materials with change in time (b is 6.25 times the magnification of Part a).

increasing CL concentration, the lignocellulosic material was the most sparse in CL-WPU98 composite film material, while

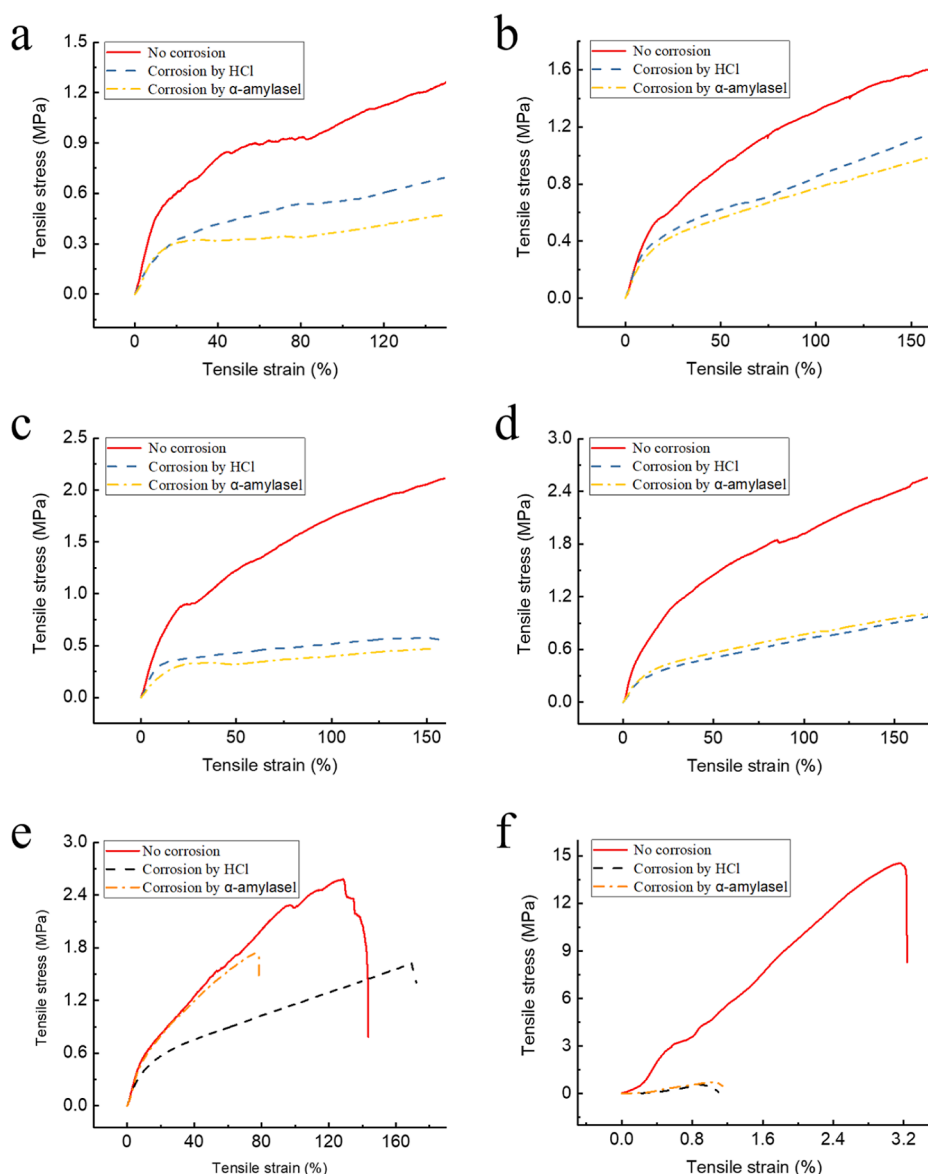


Figure 6. Influence of different etching solutions on tensile stress and strain of the CL–WPU composite membrane (a: CL–WPU98, b: CL–WPU96, c: CL–WPU94, d: CL–WPU92, e: CL–WPU90, and f: CL).

Table 1. Corrosion Resistance of Different Membrane Materials under Tensile Strain of 140%

polymer	uncorroded tensile stress (MPa)	HCl corrosion tensile stress (MPa)	α -amylase corrosion tensile stress (MPa)	HCl corrosion effect (%)	α -amylase corrosion effect (%)
CL-WPU98	1.21	0.67	0.46	44.63	61.98
CL-WPU96	1.53	1.05	0.92	31.37	39.87
CL-WPU94	2.00	0.57	0.46	71.50	77.00
CL-WPU92	2.31	0.86	0.92	62.77	60.17
CL-WPU90	2.06	1.41		31.55	
CL (maximum tensile stress)	14.55	0.10	0.48	99.31	96.70

the lignocellulosic density was the highest in CL–WPU90 composite film material.

FTIR Spectroscopic Analysis. Figure 3 shows the infrared spectra of CL–WPU composite film materials with different lignocellulosic concentrations, which is used to study the material compatibility of lignocellulosic and PU. There are strong hydroxyl absorption peaks around 3425 cm^{-1} , which are hydrogen bond stretching vibration peaks formed by $-\text{OH}$

within the CL molecule. With the increase of CL content, the absorption peaks were enhanced due to the presence of $-\text{CH}$ in CL. Both vibrational peaks appearing at $2800\text{--}3000\text{ cm}^{-1}$ are saturated alkane C–H stretching vibration peaks. The bending vibration absorption peaks of H–O–H adsorbing water molecules all appear near 1645 cm^{-1} , and the absorption peak of CL film material is obviously stronger than that of CL–WPU composite film materials because CL contains

Table 2. Relationship between λ and Concentration of WPU in CL–WPU Composite Films Materials

number	amount of enzyme added/mg	absorbance	λ/U	$\varphi/(U \cdot \text{mg}^{-1})$
standard of pipe	0	0.991	0	0
contrast of pipe	0.40	0.436	2.24	5.60
CL-WPU98	0.40	0.586	1.63	4.09
CL-WPU96	0.40	0.574	1.68	4.21
CL-WPU94	0.40	0.568	1.71	4.27
CL-WPU92	0.40	0.560	1.74	4.35
CL-WPU90	0.40	0.552	1.77	4.43
CL	0.40	0.568	1.71	4.27

–OH and has a strong ability to adsorb water molecules. There are C–N stretching vibration peaks near 1600 cm^{-1} , and N–H bending vibration absorption peaks at 1510 cm^{-1} . All film materials showed absorption peaks caused by C–H bending vibrations near 1400 cm^{-1} . In the range of $3400\text{--}3500 \text{ cm}^{-1}$, the CL–WPU wave peak becomes wider and moves to the lower wave direction compared with CL. This phenomenon also occurred with the increase of the content of water-based PU in the composite film materials, indicating that the hydroxyl group superposition between CL and water-based PU occurs with mutual association and cooperation. Figure 2 shows that no new absorption peak was generated after the composite of CL and WPU, indicating that the physical blending of CL and water-based PU only had a certain hydrogen bonding force.

Surface Hydrophilicity Analysis. As shown in Figure 4, CL-WPU98 had the largest contact angle with water of 59.05° , while CL-WPU90 had the lowest contact angle of 45.84° . With the increasing concentration of PU, the hydrophilicity of the composite membrane material became weaker, resulting in a larger contact angle with water. However, the water drops are absorbed on the surface of CL film materials less than 1 s, and the contact angle with water was 29.51° , which was much lower than that of CL–WPU composite film materials. Thus, the hydrophilicity of the film materials decreased after the modification of PU.

Water Absorption and Swelling Analysis. The swelling degree of composite film materials was measured in water absorption, and the results are shown in Figure 5. The CL film material almost stopped growing after 6 h immersion in deionized water, indicating that it slowly tended to reach the swelling equilibrium. It completely reached the swelling equilibrium completely after 9 h, at which time the equilibrium swelling degree Q_t of CL film was 88.4%. The high swelling degree of the film material is due to the large amount of hydrophilic hydroxyl groups in the CL molecules. CL–WPU composite film material tends to water absorption and swelling equilibrium at about 8 h and reaches water absorption and swelling equilibrium at about 9–10 h. With the increase of the concentration of PU in the composite films, the swelling rate of CL-WPU98 composite films was decreased, and the swelling degree of CL-WPU98 composite film was only 4.32% when it reached the absorbent swelling equilibrium. The swelling degree of CL-WPU90 composite film material reached the absorbent swelling equilibrium as high as 15.28%, which is about 3.5 times of that of CL-WPU98. This result reflects that PU has good hydrophobicity, while CL has good hydrophilicity.

Corrosion Resistance Analysis. Figure 6 and Table 1 show that the tensile strength of different film materials decreased obviously after corrosion, but the CL mass concentration of composite film material did not show a linear relationship with the tensile strength. The tensile stress of composite film material CL-WPU92 was the largest, and the tensile stress of CL-WPU90 was the largest after corrosion by HCl. The tensile stress of CL-WPU92 and CL-WPU96 were the highest after α -amylase corrosion. When the mass concentration of lignocellulosic was 10%, the elongation at break of CL-WPU90 composite films decreased the most and reached the elongation at break at 76.76% after α -amylase corrosion, and the maximum tensile stress was 1.74 MPa.

Table 1 shows that the corrosion resistance of composite films materials was improved compared with that of pure CL films materials, and CL-WPU96 had the strongest corrosion resistance. After HCl and α -amylase corrosion, the tensile stress only decreased by 31.37 and 39.87%, respectively, and the corrosion resistance of composite films materials increased by 67.94 and 56.83%, respectively, compared with that of pure CL film materials.

Enzyme Activity Analysis. The CL–WPU composite film materials with different concentrations of aqueous PU were put into the solution to study the effect on the enzyme activity, and the data are shown in Table 2. All film materials were lower than the enzyme activity of the control tube, indicating that both CL films and CL–WPU film materials had an effect on the activity of α -amylase. As the concentration of CL in the composite films increased, the enzyme activity became stronger. The enzyme activity and specific activity of the sample tube CL-WPU90 were 1.77 U and 4.43 U/mg, respectively, which were 0.06 U and 0.16 U/mg higher than the sample tube CL, although it is still lower than the enzyme activity and specific activity of the control tube. Compared with the pure CL membrane material, the biocompatibility of the CL–WPU composite membrane material has been improved.

CONCLUSIONS

1. The hydrophilicity of the CL material modified by WPU was lower than that of the pure CL film material, and the higher concentration of CL in the composite film led to a weaker hydrophilicity. The contact angle with water increased from 29.5 to 59.05° .
2. With the increase of CL concentration, tensile stress increased and tensile strain decreased. CL-WPU96 composite films showed the best corrosion resistance, and the tensile stress decreased by 28.46 and 38.66% after corrosion by HCl corrosion solution and α -amylase corrosion solution.
3. CL–WPU composite film material had better biocompatibility than RC film material. When the CL concentration reached the highest, CL–WPU composite film material had the highest α -amylase activity, which is 1.77 U, 0.06 U higher than CL film material.
4. There was only a simple physical blending between CL and water-based PU. The hydrogen bond formed between the two destroys the crystallization of the composite film material. As its crystallinity decreased, the tensile properties of the film material after being compounded with water-based PU were reduced.

AUTHOR INFORMATION

Corresponding Author

Zhenhua Xue – College of Material Science and Art Design, Key Laboratory of Inner Mongolia Autonomous Region, Inner Mongolia Agricultural University, 010018 Hohhot, China; orcid.org/0000-0002-8777-7159; Email: x_zhenhua@126.com

Authors

Haoqiang Yuan – College of Material Science and Art Design, Key Laboratory of Inner Mongolia Autonomous Region, Inner Mongolia Agricultural University, 010018 Hohhot, China
Yongqiang Zhang – College of Material Science and Art Design, Key Laboratory of Inner Mongolia Autonomous Region, Inner Mongolia Agricultural University, 010018 Hohhot, China

Complete contact information is available at:

<https://pubs.acs.org/10.1021/acsomega.2c02478>

Author Contributions

[†]H.Y. and Y.Z. are contributed equally to this work.

Notes

The authors declare no competing financial interest.

ACKNOWLEDGMENTS

This work was supported by the research Project of National Natural Science Foundation of China (31860187).

REFERENCES

- (1) Berney, T. Organ Repair and Regeneration. Eds: Giuseppe Orlando and ShafKeshavjee. London, UK: Academic Press, 2021; 289 pages. *Transpl. Int.* **2021**, *34*, 610–611.
- (2) Cave, G.; Fatehi, P. Impact of physicochemical properties of biomass-based fly ash on lignocellulose removal from pulping spent liquor. *Bioresources* **2018**, *13*, 9092–9115.
- (3) Colson, J.; Kovalcik, A.; Kucharczyk, P.; Gindl-Altmutter, W. Reinforcement of poly lactic acid with spraydried lignocellulosic material. *Bioresources* **2019**, *12*, 1112–1127.
- (4) Ezgi, M.; Ayşe, B.; Çakmen, B. A.; Sevgi, B.; Süleyman, K.; Burhan, A.; İsmet, Y. Preparation of hybrid PU/PCL fibers from steviol glycosides via electrospinning as a potential wound dressing materials. *J. Appl. Polym. Sci.* **2020**, *137*, 49217.
- (5) Fahma, F.; Hori, N.; Iwata, T.; Takemura, A. PVA nanocomposites reinforced with cellulose nanofibers from oil palm empty fruit bunches (OPEFBs). *Emir. J. Food Agric.* **2017**, *29*, 323–329.
- (6) Fan, W.; Wang, J.; Li, Z. Antiglare waterborne polyurethane/modified silica nanocomposite with balanced comprehensive properties. *Polym. Test.* **2021**, *99*, 107072.
- (7) Fuensanta, M.; Jofre-Reche, J. A.; Rodríguez-Llansola, F.; Costa, V.; Martín-Martínez, J. M. Structure and adhesion properties before and after hydrolytic ageing of polyurethane urea adhesives made with mixtures of waterborne polyurethane dispersions. *Int. J. Adhes. Adhes.* **2018**, *85*, 165–176.
- (8) Garry, D. J.; Garry, M. G. Interspecies chimeras and the generation of humanized organs. *J. Circ. Res.* **2019**, *124*, 23–25.
- (9) GB/T 1040.3 Plastics—Determination of tensile properties - Part 3: Test conditions for films and sheets; Standardization Administration of China: Beijing, China, 2006.
- (10) Ghaffari, S.; Yousefzadeh, M.; Mousazadegan, F. Investigation of thermal comfort in nanofibrous three-layer fabric for cold weather protective clothing. *Polym. Eng. Sci.* **2019**, *59*, 2032–2040.
- (11) Girouard, N.; Xu, S.; Schueneman, G.; Shofner, M.; Meredith, J. Site-selective modification of cellulose nanocrystals with isophorone diisocyanate and formation of polyurethane-CNC composites. *ACS Appl. Mater. Interfaces* **2016**, *8*, 1458–1467.
- (12) He, B.; Liu, X.; Qi, Q.; Zheng, R.; Chang, M.; Lin, Q.; Ren, J. A review of water-resistant cellulose-based materials in pharmaceutical and biomedical application. *Curr. Med. Chem.* **2021**, *28*, 8296–8318.
- (13) Huang, L.; Lee, W.; Chen, Y. Bio-based hydrogel and aerogel composites prepared by combining cellulose solutions and waterborne polyurethane. *Polymers* **2022**, *14*, 204.
- (14) Jochem, D.; Bösch, M.; Weimar, H.; Dieter, M. National wood fiber balances for the pulp and paper sector: An approach to supplement international forest products statistics. *For. Pol. Econ.* **2021**, *131*, 102540.
- (15) Paksung, N.; Pfersich, J.; Arauzo, P. J.; Jung, D.; Kruse, K. Structural effects of cellulose on hydrolysis and carbonization behavior during hydrothermal treatment. *ACS Omega* **2020**, *5*, 12210–12223.
- (16) Khlyustova, A.; Cheng, Y.; Yang, R. Vapor-deposited functional polymer thin films in biological applications. *J. Mater. Chem. B* **2020**, *8*, 6588–6609.
- (17) Kolzunova, L.; Shchitovskaya, E.; Karpenko, M. Polymethylacrylamide/AuNPs nanocomposites: Electrochemical synthesis and functional characteristics. *Polymers* **2021**, *13*, 2382.
- (18) Li, D.; Cheng, Y.; Zuo, H.; Zhang, W.; Pan, G.; Fu, Y.; Wei, Q. Dual-functional biocatalytic membrane containing laccase-embedded metal-organic frameworks for detection and degradation of phenolic pollutant. *J. Colloid Interface Sci.* **2021**, *603*, 771–782.
- (19) Lyu, Y.; Zhang, Q.; Wang, Z.; Pu, J. A graphene oxide nanofiltration membrane intercalated with cellulose nano-crystals. *Bioresources* **2018**, *13*, 9116–9131.
- (20) Magnin, A.; Entzmann, L.; Bazin, A.; Pollet, E.; Avérous, L. Green recycling process for polyurethane foams by a chem-biotech approach. *ChemSusChem* **2021**, *14*, 4234–4241.
- (21) Leila, M.; Arash, K.; Masoud, Y.; Marvdashti, L.; Koocheki, A.; Yavarmanesh, M. Release profile and antimicrobial properties of bioactive polyvinyl alcohol-Alyssum homolocarpum seed gum-nisin composite film. *Food Biophys.* **2019**, *14*, 120–131.
- (22) Mouro, C.; Dunne, C.; Gouveia, I. Designing new antibacterial wound dressings: Development of a dual layer cotton material coated with poly(vinyl alcohol) chitosan nanofibers incorporating Agrimonia eupatoria L. extract. *Molecules* **2020**, *26*, 83.
- (23) Natterodt, J. C.; Shirole, A.; Sapkota, J.; Zoppe, J. O.; Weder, C. Polymer nanocomposites with cellulose nanocrystals made by coprecipitation. *J. Appl. Polym. Sci.* **2018**, *135*, 45648.
- (24) Onat, B.; Rosales-Solano, H.; Pawliszyn, J. Development of a biocompatible solid phase microextraction thin film coating for the sampling and enrichment of peptides. *Anal. Chem.* **2020**, *92*, 9379–9388.
- (25) Panda, S.; Panda, P.; Nayak, S. K.; Mohanty, M. A review on waterborne thermosetting polyurethane coatings based on castor oil: Synthesis, characterization, and application. *Polym. Plast. Technol.* **2018**, *57*, 500–522.
- (26) Pei, A.; Malho, J.; Ruokolainen, J.; Zhou, Q.; Berglund, L. Strong nanocomposite reinforcement effects in polyurethane elastomer with low volume fraction of cellulose nanocrystals. *Macromolecules* **2011**, *44*, 4422–4427.
- (27) Qu, D.; Chu, G.; Martin, P.; Vasilyev, G.; Vilenky, E.; Zussman, E. Modulating the structural orientation of nanocellulose composites through mechano-stimuli. *ACS Appl. Mater. Interfaces* **2019**, *11*, 40443–40450.
- (28) Kittle, J.; Qian, C.; Edgar, E.; Roman, M.; Esker, R. Esker Adsorption of xyloglucan onto thin films of cellulose nanocrystals and amorphous cellulose: film thickness effects. *ACS Omega* **2018**, *3*, 14004–14012.
- (29) Seddiqi, H.; Oliaei, E.; Honarkar, H.; Jin, J.; Geonzon, L. C.; Bacabac, R. G.; Klein-Nulend, J. Cellulose and its derivatives: towards biomedical applications. *Cellulose* **2021**, *28*, 1893–1931.
- (30) Su, W.-F.; Chun, C.; Hsiang, S.; Chen, H.; Chun, H. Exceptional biocompatibility of 3D fibrous scaffold for cardiac tissue engineering fabricated from biodegradable polyurethane blended with cellulose. *Int. J. Polym. Mater. Polym.* **2016**, *65*, 703–711.

(31) Weishaupt, R.; Zünd, J.; Heuberger, L.; Zuber, F.; Faccio, G.; Robotti, F.; Ferrari, A.; Fortunato, G.; Ren, Q.; Maniura-Weber, K.; Guex, A. Sustainably sourced: Cellulose membranes with bifunctional peptides for advanced wound dressings. *Adv. Healthcare Mater.* **2020**, *9*, No. e1901850.

(32) Yuwawech, K.; Wootthikanokkhan, J.; Wanwong, S.; Tanpichai, S. Polyurethane/esterified cellulose nanocrystal composites as a transparent moisture barrier coating for encapsulation of dye sensitized solar cells. *J. Appl. Pol. Sci.* **2017**, *134*, 45010.

(33) Zhang, P.; Lu, Y.; Fan, M.; Jiang, P.; Bao, Y.; Gao, X.; Xia, J. Role of cellulose-based composite materials in synergistic reinforcement of environmentally friendly waterborne polyurethane. *Prog. Org. Coat.* **2020**, *147*, 105811.